Oscillation of a Small Hα Surge in a Solar Polar Coronal Hole

Kyung-Suk Cho[1,2] , Il-Hyun Cho[3] , V. M. Nakariakov[4,5] , Vasyl B. Yurchyshyn[6] , Heesu Yang[1] , Yeon-Han Kim[1] ,
Pankaj Kumar[7] , and Tetsuya Magara[3,4]

[1] Space Science Division, Korea Astronomy and Space Science Institute, Daejeon 305-348, Republic of Korea; kscho@kasi.re.kr
[2] Department of Astronomy and Space Science, University of Science and Technology, Daejeon 305-348, Republic of Korea
[3] Department of Astronomy and Space Science, Kyung Hee University, Yongin 17104, Republic of Korea
[4] School of Space Research, Kyung Hee University, Yongin 17104, Republic of Korea
[5] Centre for Fusion, Space & Astrophysics, Physics Department, University of Warwick, Coventry CV4 7AL, UK
[6] Big Bear Solar Observatory, Big Bear City, CA 92314-9672, USA
[7] Heliophysics Science Division, NASA Goddard Space Flight Center, Greenbelt, MD 20771, USA

Abstract

Hα surges (i.e., cool/dense collimated plasma ejections) may act as a guide for a propagation of magnetohydrodynamic waves. We report a high-resolution observation of a surge observed with 1.6 m Goode Solar Telescope (GST) on 2009 August 26, from 18:20 UT to 18:45 UT. Characteristics of plasma motions in the surge are determined with the normalizing radial gradient filter and the Fourier motion filter. The shape of the surge is found to change from a "C" shape to an inverse "C" shape after a formation of a cusp, a signature of reconnection. There are apparent upflows seen above the cusp top and downflows below it. The upflows show rising and rotational motions in the right-hand direction, with the rotational speed decreasing with height. Near the cusp top, we find a transverse oscillation of the surge, with the period of ∼2 minutes. There is no change of the oscillation phase below the cusp top, but above the top a phase change is identified, giving a vertical phase speed about 86 km s^{-1}. As the height increases, the initial amplitude of the oscillation increases, and the oscillation damping time decreases from 5.13 to 1.18 minutes. We conclude that the oscillation is a propagating kink wave that is possibly excited by the repetitive spontaneous magnetic reconnection.

Key words: magnetic reconnection – Sun: chromosphere – Sun: oscillations

Supporting material: animation

1. Introduction

Surges in Hα have been studied since their first observation by McMath & Pettit (1937). Typically, surges eject a chromospheric cold and dense plasma into the corona up to 200 Mm (Roy 1973). Surges often exhibit upward rising motion along a straight or slightly curved trajectory, and then diffuse, fade out, or fall back (Svestka 1976; Foukal 1990; Tandberg-Hanssen 1995). The speed of surges is not constant and they often exhibit acceleration/deceleration pattern (e.g., Tamenaga et al. 1973; Sakaue et al. 2018). A rotational motion around the axis of a surge has been reported by Bruzek (1974). Canfield et al. (1996) proposed that the rotation could be associated with a relaxation process (untwisting) produced by magnetic reconnection between a twisted loop and an ambient open flux tube (see also Shibata & Uchida 1986). According to the model of Yokoyama & Shibata (1996), the cool plasma can be accelerated by the slingshot effect (tension force). Most of the previous studies focus on global plasma motion in Hα surges, while plasma motion inside surges has not been investigated in detail due to the limited spatial and time resolution of available observations.

As with other chromospheric features such as filaments, fibrils, mottles, and spicules, surges act as a guide for magnetohydrodynamic (MHD) waves. Our interest in waves is connected with the role that they may play in the upper atmospheric plasma heating (e.g., Parnell & De Moortel 2012), and with their potential for seismological plasma diagnostics (e.g., Verth & Jess 2016). While there are many reports about oscillatory motions in hot plasma ejections such as extreme-ultraviolet (EUV) and X-ray jets (e.g., Chandrashekhar et al. 2014a, 2014b; Morton et al. 2012), to our knowledge only a few

reports about the cold plasma oscillation in small surges have been presented. Chae et al. (1999) suggested that EUV/X-ray jets (hot plasma) and Hα surges (cold plasma) are different kinds of ejections, but dynamically connected to each other.

In this study, we present a well-observed small scale Hα surge in the northern polar coronal hole (CH) observed by the Goode Solar Telescope (GST). Observations of the surge in the polar region under excellent seeing conditions lasting more than 10 minutes are unique because the majority of surges occur in active regions. The observed surge shows a clear bifurcation structure and slight acceleration during its rising motion, which are signatures of magnetic reconnection. A rotational motion and a transverse oscillation after the reconnection are identified. To our knowledge, this is the first report on the oscillatory properties of cold plasma in the small Hα surge observed in a polar CH. The following section describes the data and methods. In Section 3, we present dynamics of cold plasma in the surge and its oscillation. Finally, we summarize and discuss our results.

2. Data and Method

The data were obtained using the narrowband (0.5 Å) Hα Lyot filter that was installed at the Nasmyth focus of GST without an adaptive optics (AO) system. On 2009 August 26, we performed Hα observations by using a 2K by 2K charge-coupled device (CCD) from 18:20 UT to 18:45 UT with 15 s time cadence. The data set was binned by 2 × 2 with the pixel resolution of 0″07 corresponding to 51.63 km pixel^{-1}. The field of view was 61″ × 66″ after an alignment and rotation of the images.

The observed target was a small surge seen in the north polar CH at the Hα center wavelength. Because the AO system was not available in the early phase of the observation, we used the Kiepenheuer-Institute Speckle Interferometry Package (Wöger et al. 2008), which produce a speckle-reconstructed image from several short-exposed images to minimize the seeing effect. In fact, we obtained an image by applying the reconstruction technique to burst data that contained 70 images with an exposure of 50 ms.

A brief description of the basic data reduction process is described in Kim et al. (2010), who used the same data set and inspected the surge kinematics in three different phases. They reported interesting features of the surge such as a slight acceleration, untwisting motion, and oscillation. However, a quantitative analysis of the dynamics and oscillation has not been conducted. We re-inspect the surge by utilizing the same data set but applying a new analytical technique. We use a normalizing radial graded filter (NRGF; Morgan et al. 2006) to enhance the image, the Fourier motion filtering to derive a velocity field map, and a time–distance plot to quantify the oscillation.

The analysis was performed in the following steps: First, we used sub-regions around the surge from 18:32:51 UT for a ~11 minute time interval. The size of the intensity movie is $100 \times 300 \times 48$ ($7'' \times 21'' \times 48$). The NRGF is applied to the original intensity image. For a given frame, the intensity at each height is subtracted by its horizontal average and divided by its standard deviation. We then obtained a movie ($I(x, y, t)$) from a series of normalized images. This task greatly enhances the faint intensity signals at a high altitude as shown in the movie in Figure 1. The movie shows the Hα surge ejections from 18:32:51 UT to 18:44:36 UT with 15 s cadence. Snapshots of Hα surges with a 1 minute interval from 18:33:51 UT are presented in Figure 1. In the second panel, a cusp that can be taken as a signature of reconnection is clearly seen. A structure with two threads is observed in the third and fourth panels. To inspect the dynamics and oscillation of the surge, we put horizontal slits at different heights across the surge. Then, horizontal and vertical speeds in the plane of sky are determined by applying the Fourier motion filtering (e.g., DeForest et al. 2014; Cho et al. 2018) to the time series of intensity images. A phase speed filtering is performed within the speed range ($v = -100, -98, -96, ..., 100\,\mathrm{km\,s^{-1}}$) with a passband ($\sigma_v$) of 2 km s^{-1}. Finally, to identify an oscillation pattern clearly, we created a time–displacement (x–t) plot of the filtered intensity for a given height of the surge with the subtraction of global displacements in the transverse direction. The global displacement is determined by fitting the local displacement with a second-order polynomial function.

3. Results

The surge showed a two-step rising motion (i.e., slow and fast rising). The slow rise starts at 18:33 UT and erupts after forming a cusp with a rising speed about 20–30 km s^{-1}. Several interesting features such as bifurcation, rotation, and transverse oscillation can be seen in the Figure 1 animation.

3.1. Dynamics

Figure 1 shows the evolution of the surge from a "C"-shape into an inverse "C"-shape. When the shape changes, a cusp is formed clearly underneath the surge in underlying loops. As shown in the bottom panel of the figure, the surge exhibit two-step profile (slow rise and fast rise) with a rapid speed change from 14 to 28 km s^{-1} at ~18:35 UT. In the movie, the surge moves from left to right, and the rotational motion with a bifurcating structure is seen in the upper parts of the surge. It is also noted that cool plasmas are located in the left part of the cusp, and that the cool plasma structure is getting thicker during the eruption (see the last panel of Figure 1). The structure fades out after 18:42 UT.

To inspect the dynamics of the surge, we put slits at four different heights of the surge (see the last panel of Figure 1). We select these slit heights to avoid the noisy strips that are clearly seen above 200 pixel in Figure 1. Figures 2(a)–(d) shows time–distance maps constructed on those slits. As height increases, the position of the surge moves about 15 pixels (~774 km) to the right, and the first appearance time of the surge is delayed about 1 minute. Then, after 18:39:51 UT (T7), the movement turns to the left. The width of the surge does not significantly change in the lower heights ((c) and (d)) but it becomes larger after 18:37:51 UT (T5) as shown in panels (a) and (b). A twisted knot structure is seen in the panel (a) from 18:38:51 UT (T6), which may be related to the rotational motion of the surge as seen in the movie. A transverse (kink) oscillation is detected above the cusp top in Figure 1, but there are no clear oscillatory features at the other heights (see the left panels of Figure 2).

Using the Fourier motion filtering method, we investigate the plasma velocity of the surge in the plane of the sky in detail. For the region shown by the box in the upper panels of Figure 3, we estimate transverse and vertical speed distributions using the method, and plot the transverse and vertical components. The velocity field distribution of upward and downward motions is denoted with the arrows.

Before the cusp formation, there is a localized transverse motion in middle-left and lower-right parts of the C-shaped surge as denoted by arrows in panel (a1). In panel a3, the plasma motion in the rightward direction is dominant, which is likely to be associated with the formation of the inverse-C shape as well as the growth of the right leg of the cusp (b1). The lower-middle part of the surge is filled with downflows, as shown in panels (a2) and (a4). After the cusp is formed, the top of the cusp and its right leg are occupied with high-speed upward flows, while the left leg is filled with downward-moving plasma; see panels (b2) and (b4). After the appearance of the bifurcation feature on the top of the surge as shown in Figure 3(c), the diverging flows from the cusp become more clearly seen in panels (c3) and (c4). Two different upflows along the bifurcation features are identified in panel (c2). The rotational motion of the surge can be seen from the upflow velocity components in panels (b3) and (c3). After the strong upflow, the width of surge becomes larger (d) and the bidirectional motion is getting weaker (d2). Finally, the surge is occupied with downflows (e4) and the width of surge increases further (e).

3.2. Oscillation

To study the transverse oscillatory displacement of the surge in more detail, we selected four additional slits above and below slit "1," and created time–distance maps. We extract the surge region by applying the growing method (the *IDL* function
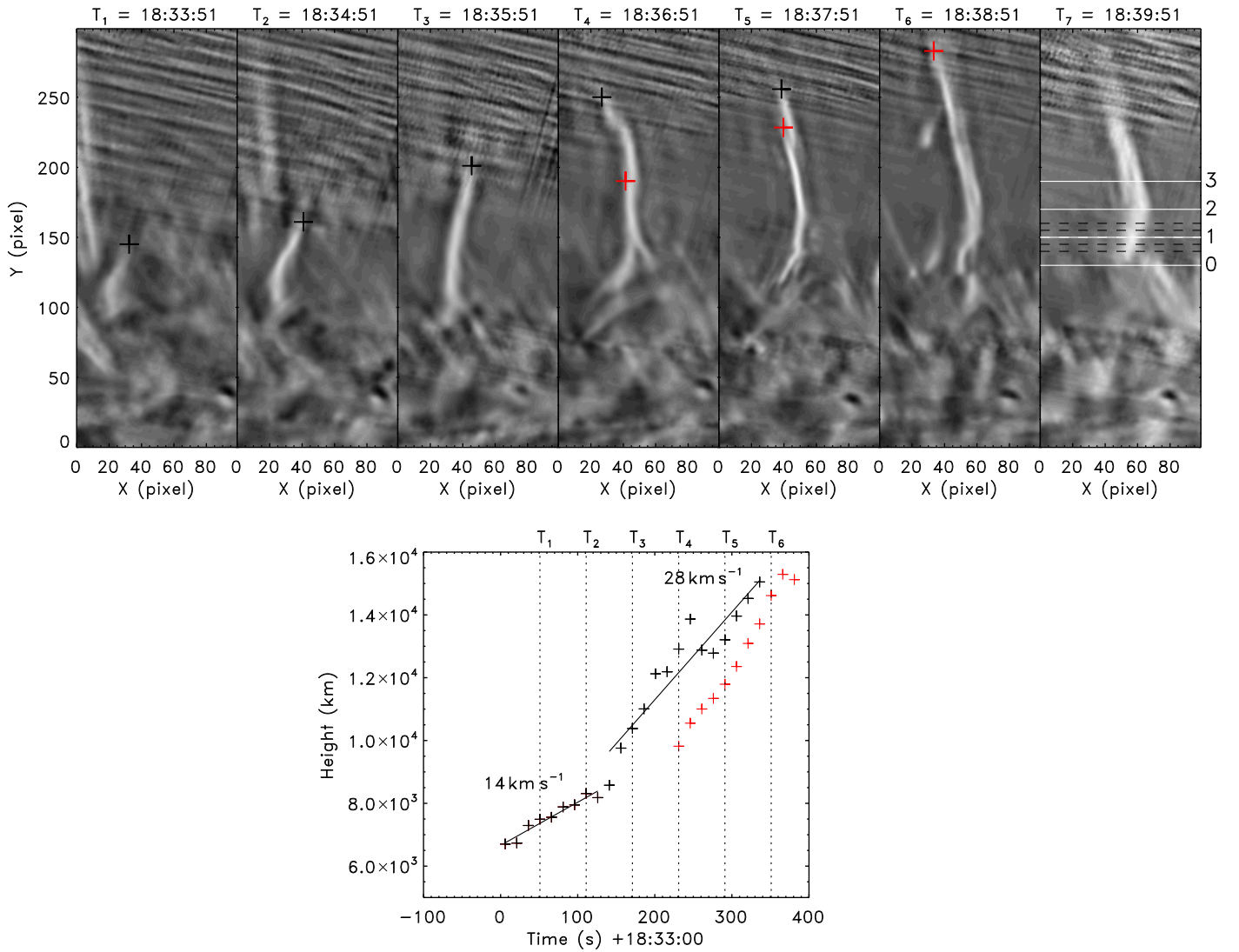
Figure 1. Snapshots (upper panels) of the Hα surge from 18:33:51 UT to 18:39:51 UT and height–time plot (bottom panel) of the surge. The black cross denotes the height of the surge, and the solid line represents linear fit of the heights. The red cross denotes a lower part of the bifurcating structure that appeared from 18:36:51 UT. The white lines in the upper right panel indicate four different heights (130, 150, 170, 190 pixels) used for the dynamics inspection, and the black dashed lines, including the slit "1" line, denote five different heights (140, 145, 150, 155, 160 pixels) used for the oscillation inspection and the time–distance maps in Figure 2. The length per pixel is ∼51.63 km pixel⁻¹. The accompanying animation of the upper panels depicts the full data set from 18:32:51 UT to 18:44:36 UT and denotes the heights of the surge with the black and red cross symbols. The video duration is 8 s.

(An animation of this figure is available.)

region_grow.pro with a threshold intensity of 1.0) to the time–distance maps of the normalized intensity. A slow displacement trend is determined by applying the least-square fitting of a second-order polynomial (Figure 4). The oscillatory displacement is determined by subtracting the trend from the central position of the surge. Clear oscillatory displacement patterns are identified at the five different heights.

Parameters of the oscillations are determined by fitting the displacement $\xi(t)$ with a function

$$\xi(t) = A_0 \exp\left[\frac{-(t - t_0)}{\tau_D}\right] \cos\left[\frac{2\pi(t - t_0)}{P}\right], \quad (1)$$

where A_0, t_0, P, and τ_D are the initial amplitude, start time, period, and damping time, respectively (Table 1). The amplitude is seen to decrease more rapidly as the height increases.

Our analysis shows that the oscillation of the surge is a transverse wave with a ∼2 minute period, which propagates upward from the reconnection site. The amplitude of the wave increases with height but decreases with time. As the height increases, the damping time decreases rapidly from 5 to 1 minute. The derived velocity amplitude increases from 4 to 9 km s⁻¹. The phase difference between the displacements at different heights indicates that the wave is propagating. The phase speed above the cusp top is ∼86 km s⁻¹, which is similar to the value observed in a Ca II jet (He et al. 2009). Interestingly, it is noted that there is no phase difference below the cusp top. Assuming the chromospheric number density of 5×10^{11} cm⁻³ above the top of the cusp, the estimated energy
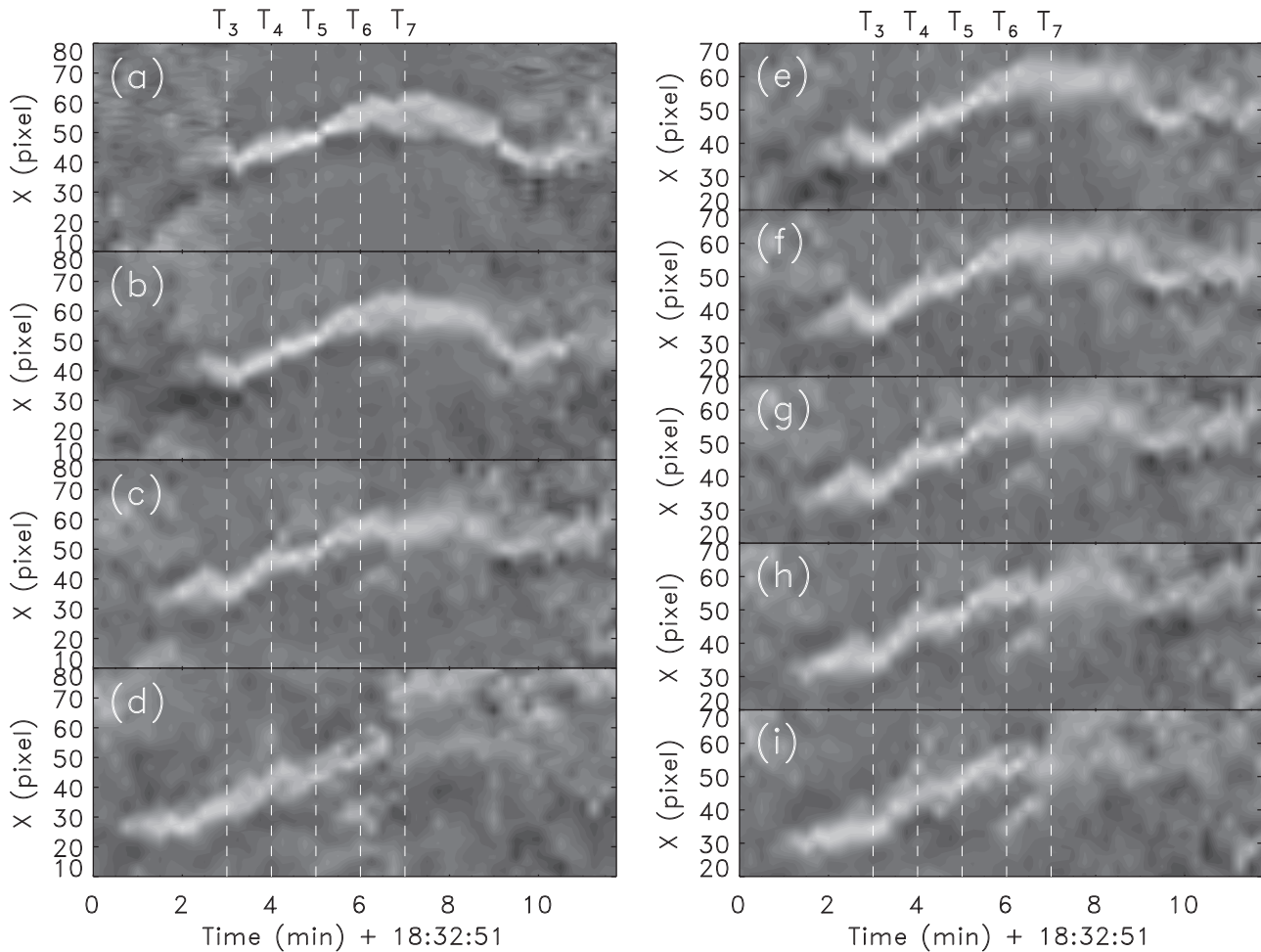
Figure 2. Time–distance maps at nine different heights denoted in Figure 1. The left panel shows time–distance maps of the Hα surge at the heights of 190 (a), 170 (b), 150 (c), 130 (d) pixels. The right panels show the time–distance maps of the surge at the heights of 160 (e), 155 (f), 150 (g), 145 (h), 140 (i) pixels. The vertical dashed lines in the panels indicate the times 3, 4, 5, 6, 7 minutes after 18:32:51 UT, respectively.

flux is $\sim 6.1 \times 10^6$ erg cm^{-2} s^{-1}. This value is not so different from that of He et al. (2009).

4. Summary and Discussion

In this study, we present an untwisting motion of an Hα surge in the north polar CH, with a transverse oscillatory motion. The presence of a cusp and two-step rising motion indicates that the surge is initiated by magnetic reconnection (Kim et al. 2010). We speculate that a microflare may occur by an interaction between an open field and small loop with the magnetic polarity that is opposite to the polarity of the CH. After the reconnection, the surge changes its shape from a "C" shape to an inverse "C" shape. There is a bidirectional plasma motion from the top of the cusp. Below the cusp, downflows become dominant after the reconnection, while the transverse motion of the plasma above the cusp is converted to an upward motion that rotates in the counter-clockwise direction. This phenomenology resembles the breakout jet scenario recently modeled by Wyper et al. (2017), and observed in EUV by Kumar et al. (2018). The inverted "Y"-shaped structure is consistent with the simulation performed for X-ray jets and Hα surges by Yokoyama & Shibata (1995) and the GST

observation by Yurchyshyn et al. (2013). These observations are consistent with the propagation of Alfvénic (kink) waves from the reconnection site as seen in chromospheric jets (Nishizuka et al. 2008).

Just above and below the cusp, we found transverse oscillatory displacements of the surge, with the average period of about 2 minutes. The period shows an apparent increase with height from 1.8 to 2.16 minutes, although it could be attributed to the errors. The oscillation behaves differently above and below the reconnection site (cusp top). Above the top of the cusp, the oscillation amplitude is strongly damped with height, and the oscillation propagates upward at the phase speed of 86 km s^{-1}. Below the top of the cusp, the oscillation phase and amplitude do not significantly change. The observed oscillation could be attributed to the repetitive spontaneous magnetic reconnection (e.g., McLaughlin et al. 2018). Indeed, numerical simulations of $m = 2$ oscillations of the magnetic null point, performed by Thurgood et al. (2017, 2019), demonstrate a similar decaying oscillatory pattern, and the detected value of the oscillation period is consistent with the numerical results. In this scenario, periodic reconnection reversals could readily excite a transverse oscillation on the reconnection jet. This interpretation opens up interesting perspectives for the
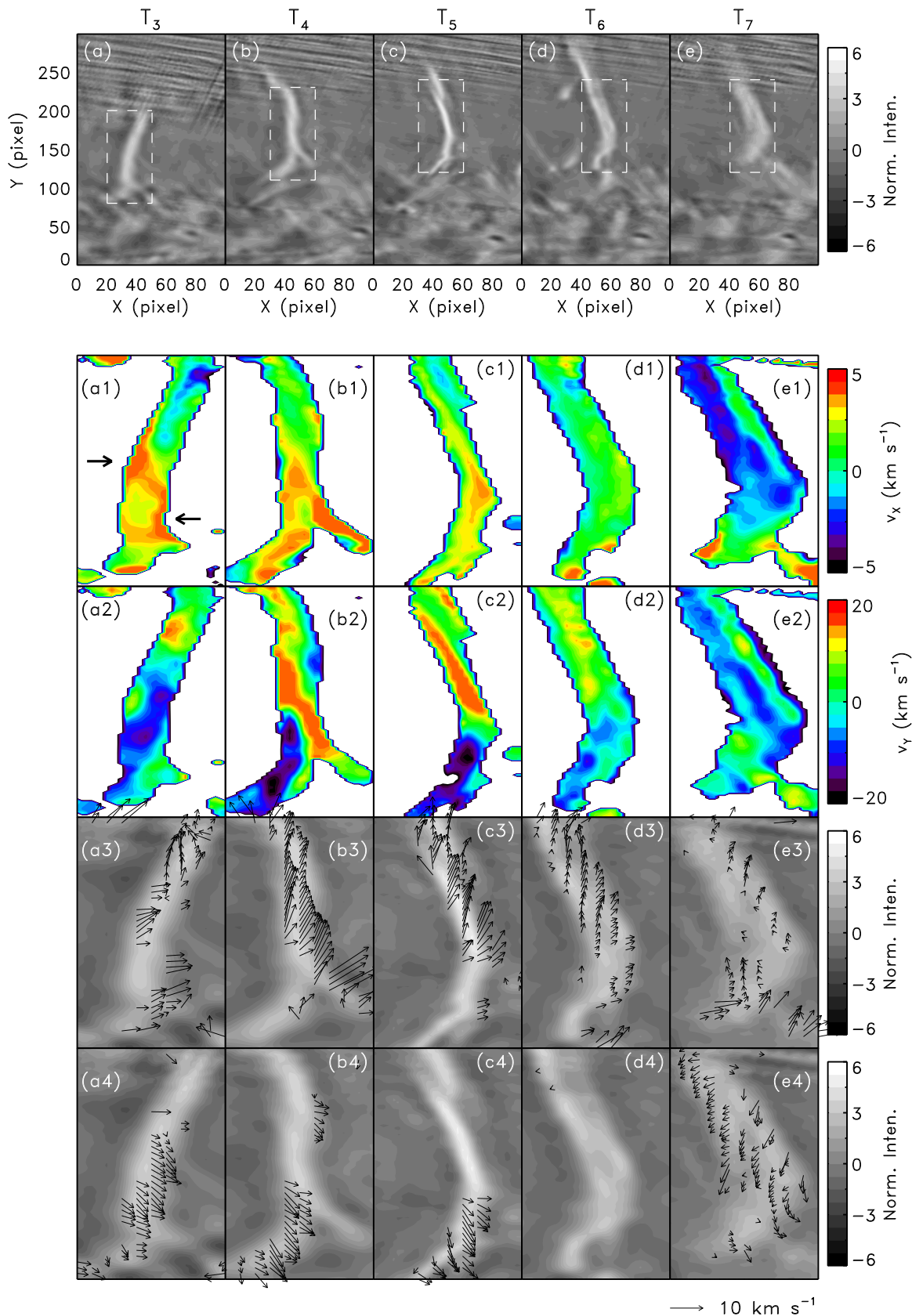
Figure 3. Snapshots of intensity (a ∼ e), transverse velocity (a1 ∼ e1), and vertical velocity (a2 ∼ e2). The 4th (a3 ∼ e3) and 5th (a4 ∼ e4) rows present velocity fields with $v_Y > 0$ (upward) and $v_Y < 0$ (downward), respectively. The dashed rectangles in the top panel denote the region of interest (ROI; 30 × 120 pixels) that covers the surge. The velocity distributions and their field maps within the ROI region are presented.
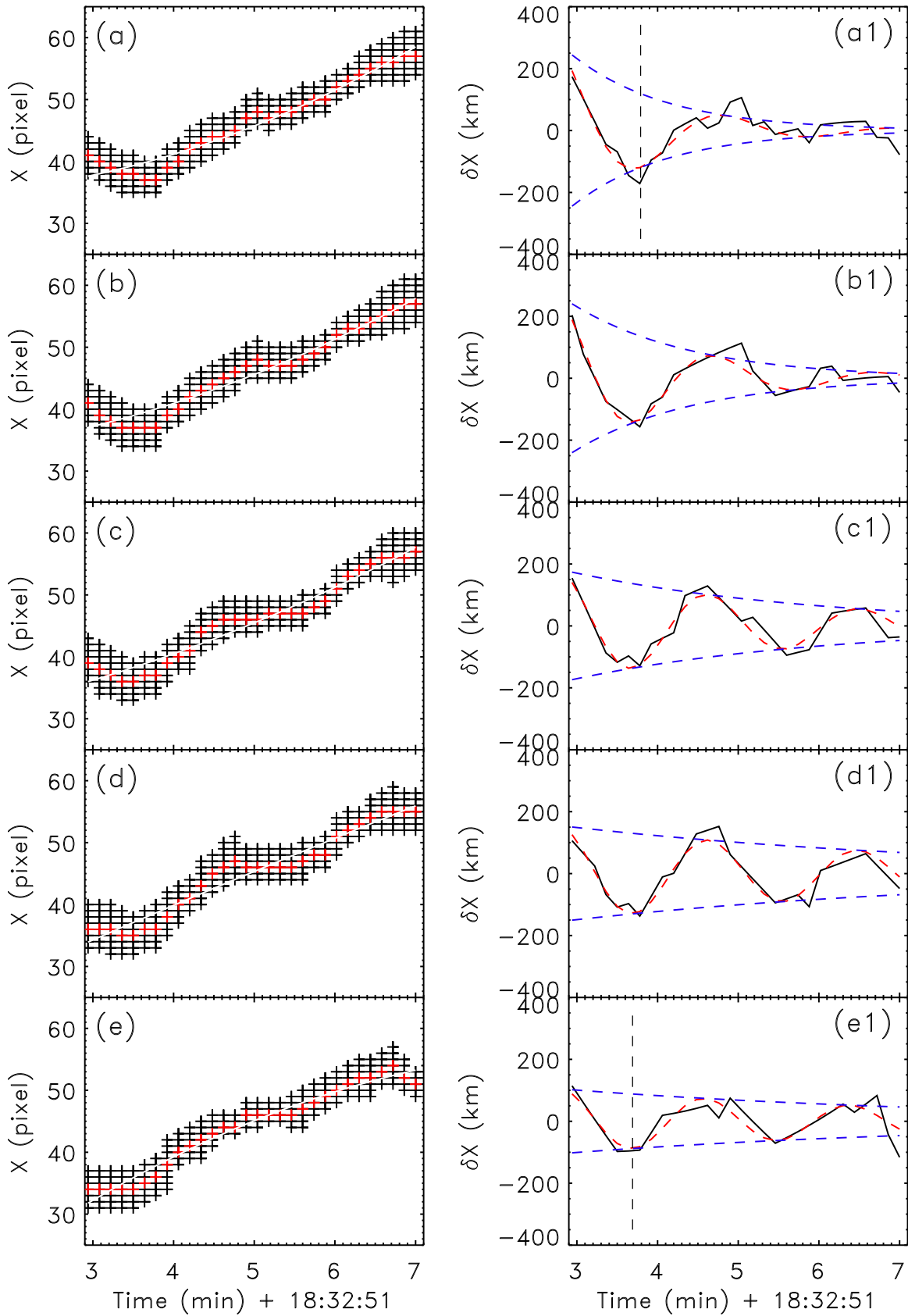
Figure 4. Temporal variations of the transverse position (a ∼ e) and its local displacement (a1 ∼ e1) of the surge at different heights (160, 155, 150, 145, and 140 pixels). The black solid lines in the right panels (a1 ∼ e1) are obtained by subtracting the second-order polynomial fit (the white line in the left panel) from the central position of the surge (the red cross in the left panel), which clearly shows oscillatory patterns. The red dashed line in the right panels is the least-square fit with the function $A_0 e^{-(t-t_0)/\tau_D} \cos(2\pi(t-t_0)/P)$. The blue dashed line denotes the envelopes derived by the exponential component of the function. The vertical dotted lines in panels (a1) and (e1) denote the first minimums of the fitting curve derived by using the function.

Table 1
Properties of Transverse Oscillations of the Surge

Height (pixel)	H (km)	A_0 (km)	P (minutes)	$t_0+P/2$ (minutes)	τ_D (minutes)	δv (km s^{-1})	v_{ph} (km s^{-1})
160	1033	295	2.16	3.79	1.18	9.13	⋯
155	774	277	2.01	3.73	1.48	9.21	86
150	516	185	1.88	3.69	3.11	6.54	⋯
145	258	156	1.86	3.70	5.13	5.58	0
140	0	105	1.80	3.69	5.13	3.89	⋯

Note. The first and second columns are heights of the slits (black dotted lines in Figure 2) in units of pixel and kilometer. We set the slit "1" height as the middle (150 pixels) height of the oscillations. The third and fourth columns give the initial amplitude and period. The fifth column shows the time of the first minimum displacement. The sixth column gives the damping time. Columns 7 and 8 are the velocity amplitude ($\delta v \sim 4A_0/P$) and the phase speed, respectively.

seismological diagnostics of the reconnection plasmas, proposed in Thurgood et al. (2019).

ORCID iDs

Kyung-Suk Cho https://orcid.org/0000-0003-2161-9606
Il-Hyun Cho https://orcid.org/0000-0001-7514-8171
V. M. Nakariakov https://orcid.org/0000-0001-6423-8286
Vasyl B. Yurchyshyn https://orcid.org/0000-0001-9982-2175
Heesu Yang https://orcid.org/0000-0001-5455-2546
Yeon-Han Kim https://orcid.org/0000-0001-5900-6237
Pankaj Kumar https://orcid.org/0000-0001-6289-7341
Tetsuya Magara https://orcid.org/0000-0003-2953-0323

References

Bruzek, A. 1974, in IAU Symp. 57, Coronal Disturbances, ed. G. A. Newkirk (Boston: Reidel), 323
Canfield, R. C., Reardon, K. P., Leka, K. D., et al. 1996, ApJ, 464, 1016
Chae, J., Qiu, J., Wang, H., & Goode, P. R. 1999, ApJL, 513, L75
Chandrashekhar, K., Bemporad, A., Banerjee, D., Gupta, G. R., & Teriaca, L. 2014a, A&A, 561, A104
Chandrashekhar, K., Morton, R. J., Banerjee, D., & Gupta, G. R. 2014b, A&A, 562, A98
Cho, I.-H., Moon, Y.-J., Nakariakov, V. M., et al. 2018, PhRvL, 121, 075101
DeForest, C. E., Howard, T. A., & McComas, D. J. 2014, ApJ, 787, 124
Foukal, P. 1990, Solar Astrophysics (New York: Wiley-Interscience), 1990
He, J., Marsch, E., Tu, C., & Tian, H. 2009, ApJL, 705, L217
Kim, Y.-H., Park, Y.-D., Bong, S.-C., Cho, K.-S., & Chae, J. 2010, in Proc. 20th National Solar Physics Meeting, ed. C. I. Dorotoviv (Hurbanovo: Slovak Central Observatory)
Kumar, P., Karpen, J. T., Antiochos, S. K., et al. 2018, ApJ, 854, 155
McLaughlin, J. A., Nakariakov, V. M., Dominique, M., Jelínek, P., & Takasao, S. 2018, SSRv, 214, 45
McMath, R. R., & Pettit, E. 1937, ApJ, 85, 279
Morgan, H., Habbal, S. R., & Woo, R. 2006, SoPh, 236, 263
Morton, R. J., Verth, G., McLaughlin, J. A., & Erdélyi, R. 2012, ApJ, 744, 5
Nishizuka, N., Shimizu, M., Nakamura, T., et al. 2008, ApJL, 683, L83
Parnell, C. E., & De Moortel, I. 2012, RSPTA, 370, 3217
Roy, J. R. 1973, SoPh, 28, 95
Sakaue, T., Tei, A., Asai, A., et al. 2018, PASJ, 70, 99
Shibata, K., & Uchida, Y. 1986, SoPh, 103, 299
Svestka, Z. 1976, Solar Flares (Berlin: Springer), 415
Tamenaga, T., Kureizumi, T., & Kubota, J. 1973, PASJ, 25, 447
Tandberg-Hanssen, E. 1995, The Nature of Solar Prominences, Astrophysics and Space Science Library, Vol. 199 (Dordrecht: Kluwer)
Thurgood, J. O., Pontin, D. I., & McLaughlin, J. A. 2017, ApJ, 844, 2
Thurgood, J. O., Pontin, D. I., & McLaughlin, J. A. 2019, A&A, 621, A106
Verth, G., & Jess, D. B. 2016, GMS, 216, 431
Wöger, F., von der Lühe, O., & Reardon, K. 2008, A&A, 488, 375
Wyper, P. F., Antiochos, S. K., & DeVore, C. R. 2017, Natur, 544, 452
Yokoyama, T., & Shibata, K. 1995, Natur, 375, 42
Yokoyama, T., & Shibata, K. 1996, PASJ, 48, 353
Yurchyshyn, V., Abramenko, V., & Goode, P. 2013, ApJ, 767, 17